Effects of GBFS content and curing methods on the working performance and microstructure of ternary geopolymers based on high-content steel slag

Yang, Xinkui; Wu, Shaopeng; Xu, Shi; Chen, Boyu; Chen, Dongyu; Wang, Fusong; Jiang, Jian; Fan, Lulu; Tu, Liangliang

DOI
10.1016/j.conbuildmat.2023.134128

Publication date
2023

Document Version
Final published version

Published in
Construction and Building Materials

Citation (APA)
Yang, X., Wu, S., Xu, S., Chen, B., Chen, D., Wang, F., Jiang, J., Fan, L., & Tu, L. (2023). Effects of GBFS content and curing methods on the working performance and microstructure of ternary geopolymers based on high-content steel slag. *Construction and Building Materials*, *410*, Article 134128. https://doi.org/10.1016/j.conbuildmat.2023.134128

Construction and Building Materials 410 (2024) 134128

Contents lists available at ScienceDirect

Construction and Building Materials

journal homepage: www.elsevier.com/locate/conbuildmat

Effects of GBFS content and curing methods on the working performance and microstructure of ternary geopolymers based on high-content steel slag

Xinkui Yang [a], Shaopeng Wu [a,*], Shi Xu [b,c], Boyu Chen [c], Dongyu Chen [a], Fusong Wang [d], Jian Jiang [e], Lulu Fan [e], Liangliang Tu [e]

[a] State Key Laboratory of Silicate Materials for Architectures, Wuhan University of Technology, Wuhan 430070, China
[b] School of Civil Engineering and Architecture, Wuhan University of Technology, Luoshi Road 122, Wuhan 430070, China
[c] Faculty of Civil Engineering and Geosciences, Delft University of Technology, Stevinweg 1, 2628 CN Delft, the Netherlands
[d] School of Civil and Hydraulic Engineering, Huazhong University of Science and Technology, Wuhan 430074, China
[e] Shenzhen Sez Construction Group Co., Ltd, Shenzhen 518034, Guangdong, China

ARTICLE INFO

Keywords:
Geopolymer
Steel slag
Working performance
Curing methods

ABSTRACT

Aimed to address the low utilization rate of steel slag (SS) and its challenge in resource utilization in China, this study developed ternary geopolymers made by high-content (50%) SS together with fly ash (FA) and granulated blast furnace slag (GBFS). The effects of GBFS content (0–40%) and curing methods (water curing, standard curing, sealed curing, and heat curing) on the working performance and microstructure of geopolymers were investigated. Microscopic analysis such as X-ray diffraction (XRD), Fourier-transform infrared spectroscopy (FTIR), thermogravimetric analysis (TG-DTG), and scanning electron microscopy (SEM) were utilized to investigate the hydration process and products of geopolymers under different curing conditions and GBFS content. The results indicated that when the GBFS content increased from 0% to 40%, the fluidity of the mixture decreased by 11.7%, the initial setting time of the geopolymer slurry decreased by 76%, and the geopolymer mortar's 28d compressive strength increased from 31.9 MPa to 60.6 MPa. At room temperature, the geopolymer mortar's 28d compressive strength was higher under standard curing (70.8 MPa) compared to water curing (57.5 MPa) and sealed curing (68 MPa). The geopolymer mortar cured at 60 °C for 24 h exhibited the highest 28d compressive strength (76.3 MPa). However, excessively high curing temperatures or prolonged durations led to more shrinkage cracks and reduced the compressive strength. The microscopic analysis revealed that the main gel products of ternary geopolymer were C-(A)-S-H gel. The amount of gel products is directly related to the strength of geopolymers. The developed ternary geopolymer has the potential to promote the large-scale utilization of SS in the concrete industry, making a significant contribution to sustainable development.

1. Introduction

Geopolymers are sustainable cementitious materials formed by inorganic polymerization of silica-aluminum constituents under activation of alkaline solution, and contain the three-dimensional network structure connected by silicon and aluminum oxygen tetrahedron [1,2]. Compared with cement, the use of geopolymers as cementitious materials has advantages for economy and environment as well as better early strength and impermeability [3].

As a kind of solid waste, fly ash (FA) has been widely used to replace cement to produce concrete. Golewski's team investigated the effect of FA on the workability and microstructure of concrete [4–7]. They found that replacing 30% of cement with FA improved the pore distribution of concrete, reduced its water absorption, thereby enhancing the structural stability of concrete under submerged conditions. In addition, to better understand the mechanical behavior of FA modified concrete, many studies have reported the use of mathematical models to predict the compressive strength of FA modified concrete [8–12]. Ahmed et al. established mathematical models based on Artificial Neural Network (ANN), M5P-Tree, Linear Regression and Multi-logistic regression models to predict the compressive strength of FA-based geopolymer concrete [13]. The results indicated that the ANN model demonstrated superior predictive capabilities. The predictions revealed that the alkali activator content and FA content significantly influenced the

* Corresponding author.
E-mail address: wusp@whut.edu.cn (S. Wu).

https://doi.org/10.1016/j.conbuildmat.2023.134128
Received 18 September 2023; Received in revised form 3 November 2023; Accepted 7 November 2023
Available online 21 November 2023

compressive strength of geopolymer concrete. Kakasor Ismael Jaf et al. employed the Interaction (IN) model to predict the impact of the SiO_2/CaO ratio on the compressive strength of FA-based geopolymer concrete [14]. The results showed that the compressive strength decreased as the SiO_2/CaO ratio increased from 0.984 to 17. However, when the ratio exceeded 17, the compressive strength increased.

However, due to the high silico-aluminous constituents in FA, it can also serve as the primary precursor materials for the synthesis of geopolymers [15,16]. Similarly, geopolymers provide a high-value re-utilization route of the solid wastes that contained silico-aluminous constituents, such as red mud and coal gangue [17,18]. To this aim, numerous studies on the development of geopolymers have been carried out using these solid waste resources [19]. Bai et al. prepared high-strength geopolymers under thermal curing conditions using red mud and FA as precursors [20]. After a 24-hour curing period at 60 °C, the geopolymer's 28d compressive strength exceeded 50 MPa. Guo et al. prepared geopolymer grouting materials using coal gangue and FA [17]. The material had the characteristics of short setting time, good durability and impermeability. Majdoubi et al. used phosphogypsum to prepare phosphate-based geopolymers [21]. The addition of phosphogypsum made the microstructure of geopolymers denser, thereby enhancing the mechanical properties of geopolymer.

Steel slag (SS) is the by-product generated during the production of steel. Dicalcium silicate (C_2S), tricalcium silicate (C_3S) and RO phase are the main components of SS [22]. Notably, China's annual SS production reached 137 million tons in 2022. Despite this magnitude, its utilization rate remains below 30% [23–25]. The accumulation and landfilling of SS not only occupy a significant amount of land resources but also pose a substantial risk of heavy metal ions leaching [26,27]. To avert such concerns, SS emerges as a viable option for serving as supplementary cementitious materials to elevate the utilization of SS and reduce energy consumption of cement industry [27,28]. However, due to the complete crystallization of minerals and the high content of inert components (such as RO phase) in SS, its cementitious activity is limited, thereby reducing the application potential of SS as cementitious material [29–32].

Some studies were conducted to explore the use of SS for preparing geopolymers. Guo and Yang prepared high-toughness geopolymers using FA and SS [33]. The results show that when the SS content was 21%, the tensile properties of geopolymers were enhanced, and the cracks generated by tensile strain was reduced. Bai et al. investigated the impact of SS on the mechanical properties of geopolymer prepared by metakaolin [34]. The geopolymer's early strength development was accelerated as the SS content improved to 10%, and the 28d flexural strength rose by 8%. Song et al. used SS to replace FA with high calcium content to prepare SS-FA binary geopolymer [35]. According to their findings, substituting SS for 20% of FA could increase the binary geopolymer's compressive strength and inhibit the formation of matrix shrinkage cracks. However, due to the inert components in SS and its relatively low content of silica-alumina components, the excessive use of SS may reduce the performance of geopolymers, resulting in long setting time and poor early strength [33,36]. Therefore, the content of SS in geopolymers is difficult to reach a high level (more than 40%), which hinders the large-scale application of SS in geopolymers.

Numerous studies have demonstrated that increasing the Ca^{2+} content in raw materials may be an effective approach to increase the geopolymers' early strength [37,38]. Granulated blast furnace slag (GBFS), which is a kind of solid waste produced by the steel industry, not only has high calcium content but also contains a certain amount of SiO_2 and Al_2O_3. Consequently, it can be used to activate the geopolymerisation and improve the mechanical properties of geopolymers [39]. Saha and Rajasekaran added GBFS to FA-based geopolymer to enhance its early strength and shortened its setting time [40]. Zakira et al. used GBFS and red mud to prepare geopolymers [41]. When the mixing ratio of GBFS and red mud was 1:1, the geopolymer has the highest 28d compressive strength at 65.7 MPa. Hongqiang et al. investigated the influence of GBFS on the strength of geopolymers made from coal gangue [42]. They found that the compressive strength of geopolymers was greatly enhanced by GBFS; at 40% GBFS content, the strength increased by 59.08%.

Geopolymers' early strength development is also significantly influenced by the curing methods [43,44]. The most common ambient-curing methods include standard curing, water curing, sealed curing and dry curing [45–48]. However, in recent years, some studies have reported that the early strength of geopolymers can be enhanced by heat curing and microwave curing. Guan et al. used microwave curing to prepare FA-based geopolymers [49]. After microwave curing for 15 min, geopolymer mortars had the compressive strengths greater than 50 MPa. Gultekin and Ramyar prepared perlite-FA geopolymers by oven curing [50], the results showed that oven curing made the microstructure of geopolymers denser, resulting in a significant improvement in early strength. Dong et al. prepared spodumene tailings-based geopolymers through the synergism of oven curing and microwave curing [51]. The geopolymers' compressive strength exceeded 200 MPa and it exhibited good freeze-thaw stability after oven curing and microwave curing.

In summary, incorporating GBFS into precursors or optimizing the curing methods may help to enhancing the performance of SS-based geopolymers. However, the current studies on geopolymers are mostly based on metakaolin, FA and GBFS, and the use of high-content SS is limited. To investigate how high-content SS interacts with other solid waste in geopolymers and how different curing methods influence the performance of high-content SS-based geopolymers, this study used SS, FA and GBFS as the precursors to prepare geopolymers, and the dosage of SS was raised to 50%. The mixing, preparation, curing and testing process of geopolymers are shown in Fig. 1. The influence of GBFS content and curing methods (water curing, standard curing, sealed curing and heat curing) on the fluidity, setting time and compressive strength of geopolymers were studied. The geopolymers prepared by different ratios and curing methods were characterized by X-ray diffraction (XRD), Fourier-transform infrared spectroscopy (FTIR), thermogravimetric analysis (TG-DTG), scanning electron microscopy (SEM) and energy dispersive spectrometer (EDS) to investigate the microstructure and reaction process of SS-FA-GBFS ternary geopolymer. This study explores the feasibility of utilizing high-content SS in geopolymers and comprehensively considers the effect of GBFS content and curing methods on the working performance and microstructure of high-content SS based ternary geopolymers. The study results provide a theoretical basis for the large-scale utilization of SS in the concrete industry.

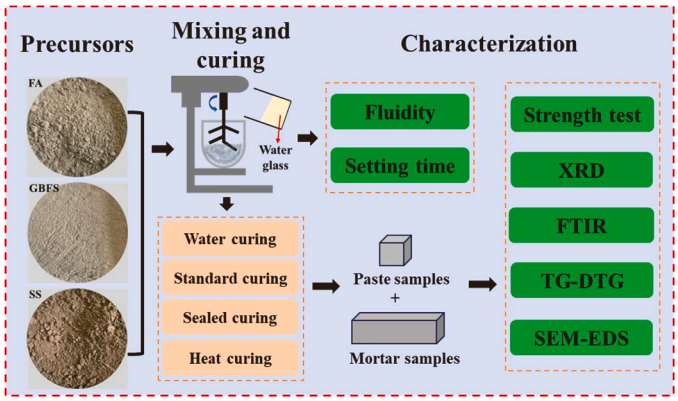

Fig. 1. Research flow chart.

2. Materials and methods

2.1. Materials

As precursors for preparing geopolymers, FA, GBFS, and SS were used. SS and GBFS were obtained from China Baowu Steel Group Co., Ltd., while FA was sourced from a power plant in Wuhan. The three solid wastes' particle size distribution was shown in Fig. 2. The average particle sizes of FA, GBFS and SS are 11.57 μm, 33.03 μm and 63.52 μm, respectively. The relatively small particle sizes of the three precursors are beneficial for increasing their reactivity [52].

X-ray fluorescence (XRF) was used to investigate the oxide composition of FA, GBFS and SS, as displayed in Table 1. FA primarily consists of SiO_2 and Al_2O_3, which make up 87.71% of the total components. GBFS is mainly composed of CaO and SiO_2, accounting for 72.64% of the total components. SS contains significant amounts of CaO and Fe_2O_3, making up 71.53% of the total components. The Si^{2+} and Al^{3+} in geopolymers primarily come from FA, while Ca^{2+} is mainly contributed by GBFS and SS. Since SS is the by-product of steel industry, Compared to FA and GBFS, the amount of Fe_2O_3 in SS is much higher. The XRD examination of the three precursors is depicted in Fig. 3. The results show that the main crystal phases in FA are mullite, quartz and calcium oxide. C_3A, C_3S, C_2S, FeO and RO phases are the main crystal phases in SS. GBFS is produced by the rapid cooling of slag produced by blast furnace ironmaking, and its composition structure is mostly glass phase, which is shown as the distribution of broad bump from $2\theta = 25^\circ$ to $2\theta = 35^\circ$ on the XRD curve.

The alkaline activator for precursors was water glass, and its basic properties are shown in Table 2. Sodium hydroxide (NaOH) was used to reduce the water glass's modulus from 3.26 to 1.5. After adding NaOH to the water glass, it needs to be stirred for 24 h to ensure the stability of modulus. The weight of NaOH added when adjusting the modulus of water glass is calculated according to the following equation:

$$m_{NaOH} = 2M_{r1}\left(\frac{m_{WG}\cdot P_{SiO_2}}{100M_{r2}\cdot M_1} - \frac{m_{WG}\cdot P_{SiO_2}}{100M_{r2}\cdot M_0}\right) \quad (1)$$

Where m_{NaOH} is the weight of NaOH (g), M_{r1} is the relative molecular mass of NaOH, m_{WG} is the weight of water glass (g), P_{SiO2} is the content of SiO_2 in water glass (wt%), M_{r2} is the relative molecular mass of SiO_2, M_1 is the target modulus of water glass, M_0 is the initial modulus of water glass.

2.2. Mix proportions, sample preparation and curing conditions

Table 3 displays the raw material mixture ratio and the curing methods. To improve the utilization rate of steel slag without reducing the performance of geopolymers, the amount of SS was set to 50% of the total weight of the precursors with a 0.5 water-binder ratio to be used. The water content already existing in the water glass was deducted when determining the amount of water to be added. As indicated in references [17,43], increasing the dosage of alkali activators leads to a higher content of Na_2O in geopolymer slurry, which will enhance the mechanical properties of geopolymers. However, excessively high dosages of alkali activators will raise the raw material costs, significantly diminishing the economic viability of geopolymers. Therefore, the Na_2O content was set to 12% of the total weight of the precursor. The amount of water glass is calculated based on the Na_2O content according to the following equation:

$$m_1 = \frac{12m_P}{P_{Na_2O}} \quad (2)$$

Where m_1 is the amount of water glass (g), m_P is the total weight of the precursors (g), and P_{Na2O} is the content of Na_2O in the water glass (wt%).

For the compressive strength and fluidity tests, mortar samples were used, whereas paste samples were used for the setting time test, XRD test, TG-DTG test, FTIR test and SEM-EDS test.

A total of 13 groups of geopolymer samples were prepared. The variables of group 1 to group 5 were set to GBFS content. The variables of group 4, group 6, group 7 and group 9 were set to the curing methods. The variables of group 8 to group 13 were set to the temperature and duration of heat curing.

In the preparation of samples, FA, GBFS and SS were fully mixed with standard sand according to the ratio in Table 3, and then water glass and water were added and stirred evenly. The 40 × 40 × 160 mm^3 mold was filled with the fresh slurry. After 2 min of vibration, the mold was wrapped in the plastic film and placed in the curing room (20 ± 2 °C, 50 ± 5% RH) for 24 h. The paste samples were prepared by the mold with a size of 40 × 40 × 40 mm^3. The mortar and paste samples precured for 24 h were taken out and continue curing in different conditions according to Table 3. As shown in Fig. 4, different curing methods were carried out by the following steps:

(1) Water curing: The mortar and paste samples were immersed in water and placed in the curing room, The spacing between the samples exceeds 10 cm.

(2) Standard curing: the mortar and neat paste samples were directly placed in the curing room.

(3) Sealed curing: the mortar and paste samples were wrapped with plastic film and placed in the curing room.

(4) Heat curing: The samples of mortar and paste were placed in the oven after being wrapped in plastic film. After curing at different temperatures for the corresponding time, the plastic film was removed and the samples were placed in the curing room to continue curing.

In engineering applications, standard curing is suitable for the curing of geopolymer concrete prefabricated parts, while water curing and sealed curing are suitable for most engineering scenarios due to their simple operation. Heat curing is suitable for scenarios with higher requirements for the early strength of geopolymer concrete.

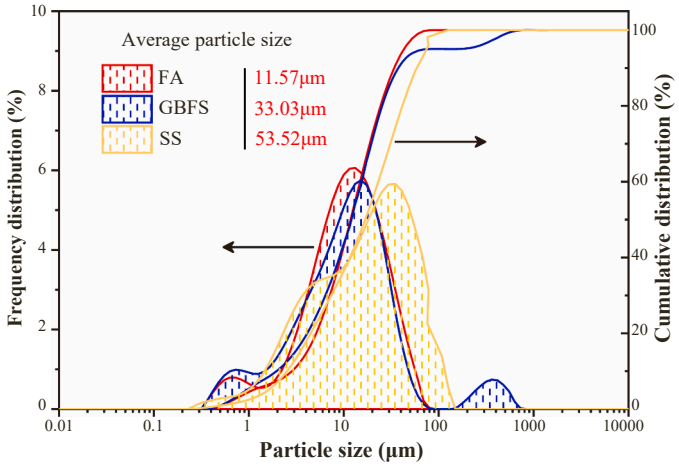

Fig. 2. Particle size distribution of FA, GBFS and SS.

2.3. Testing methods

2.3.1. Working performance

2.3.1.1. Fluidity of mortar. To evaluate how GBFS content affects the fluidity of geopolymers, the fluidity test was conducted based on Chinese standard GB/T 2419–2005. The fresh mortar was poured into the conical mold with a top diameter of 70 mm, bottom diameter 100 mm and height 60 mm. The mold was taken out upwards after the mortar is fully filled with the mold. After 25 times of vibration on the jumping platform, the flow diameter of the mortar is measured as the value of fluidity. Each mixture was measured four times and an average with standard deviation was reported.

Table 1
Oxide composition of FA, GBFS and SS.

Raw materials	Oxide type	CaO	SiO_2	Al_2O_3	MgO	Fe_2O_3	Na_2O	K_2O	P_2O_5	MnO
FA	Oxide content (%)	2.44	54.90	32.81	0.96	3.04	0.70	1.77	0.19	0.03
GBFS		40.42	32.22	15.00	7.40	0.48	0.38	0.47	0.03	0.16
SS		45.40	11.80	1.94	3.85	26.13	0.17	0.12	1.94	2.94

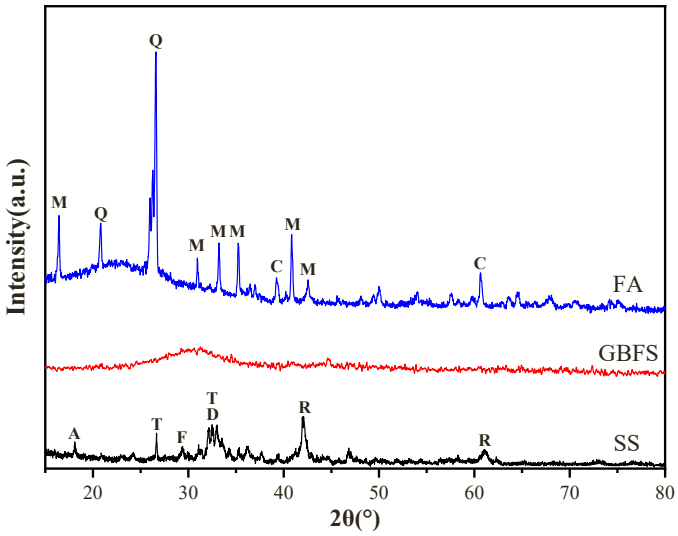

Fig. 3. XRD patterns of FA, GBFS and SS, M=Mullite, Q=Quartz, C=CaO, A=C_3A, T = C_3S, F=FeO, D=C_2S, R=RO Phase.

Table 2
Basic properties of water glass.

Properties	Value
Baume degrees	38.5
Modulus	3.26
Solid content/%	35.5
Na_2O content/%	8.53
SiO_2 content/%	26.98

2.3.1.2. Setting time. For the application of geopolymers in engineering, the setting time is essential. According to the Chinese standard GB/T 1346–2011, the setting time of GW0, GW10, GW20, GW30 and GW40 were tested by a Vicat instrument. The Vicat needle with a length of 50 ± 1 mm and a diameter of 1.13 ± 0.05 mm was used for testing the initial setting time. The Vicat needle with a length of 30 ± 1 mm, a diameter of 1.13 ± 0.05 mm and a circular cutting edge at the top was used for testing the final setting time. The measurement was taken every 30 min before the initial setting time and then shortened to every 2 min when approaching the initial and final setting time. Each mixture was measured three times and an average with standard deviation was reported.

2.3.1.3. Compressive strength. According to the Chinese standard GB/T 17671–2021, the 3d, 7d and 28d compressive strength of mortar samples were tested by the electronic universal testing machine (Yixuan TYE-3000, China). The loading speed of the pressure is set to 2.4 kN/s. Mortar samples of each ratio were measured six times and an average with standard deviation was reported.

The laboratory photos of the working performance test of the geopolymer samples are shown in Fig. 5.

2.3.2. Microscopic analysis

After crushing the paste samples, to inhibit hydration, the central part of the sample was submerged in anhydrous ethanol for 7 days. After that, the sample was dried for 24 h at 40 °C in a vacuum drying oven to get rid of any remaining anhydrous ethanol. The dried samples were pulverized into powders with a particle size of less than 0.075 mm for XRD test, TG-DTG test and FTIR test. The microstructure and reaction products of paste samples were investigated by SEM (Zeiss Gemini 300, Germany). The scanning speed of the XRD (Rigaku Dmax-2500PC, Japan) is 2°/min, from 2θ= 5° to 2θ= 65°. The heating rate of the thermogravimetric analyzer (Netzsch TMA402F3, Germany) is set to 10 °C/min, and the temperature is increased from 0 °C to 1000 °C. The detection wavenumber of infrared spectrometer (Delite DH108, China) is set to 400–4000 cm^{-1}. Before the EDS test, the central part of the paste sample was cured with epoxy resin, and then polished with 200 mesh, 400 mesh, 800 mesh, 1200 mesh, 2000 mesh and 4000 mesh sandpaper respectively, and finally polished with 3 μm polishing fluid. The aim is to grind off the unhydrated particles on paste samples' surface so as to observe the distribution of different phases. Finally, a layer of platinum is plated on the surface of the sample to improve the imaging quality.

Table 3
The mixing ratio of raw materials and the curing conditions of samples.

Group number	Group code	Solid waste content/% by total weight of precursors			Curing method
		SS	FA	GBFS	
1	GW0	50	50	0	20 ± 2 °C, Water curing
2	GW10	50	40	10	20 ± 2 °C, Water curing
3	GW20	50	30	20	20 ± 2 °C, Water curing
4	GW30	50	20	30	20 ± 2 °C, Water curing
5	GW40	50	10	40	20 ± 2 °C, Water curing
6	GST30	50	20	30	20 ± 2 °C, Standard curing
7	GS30	50	20	30	20 ± 2 °C, Sealed curing
8	GH30_40C_24 h	50	20	30	40 °C for 24 h, Heat curing
9	GH30_60C_24 h	50	20	30	60 °C for 24 h, Heat curing
10	GH30_80C_24h	50	20	30	80 °C for 24 h, Heat curing
11	GH30_60C_6 h	50	20	30	60 °C for 6 h, Heat curing
12	GH30_60C_12 h	50	20	30	60 °C for 12 h, Heat curing
13	GH30_60C_18 h	50	20	30	60 °C for 18 h, Heat curing

Group code (Example): GH30_40C_24 h: 30% GBFS content and heat curing under 40 °C for 24 h.

3. Results and discussion

3.1. Working performance of geopolymer

3.1.1. Fluidity

Fig. 6 shows the relationship between the fluidity and the GBFS content. It is evident that the fluidity of the geopolymers was decreased by the addition of GBFS. As the GBFS content increased to 40%, the fluidity decreased by 11.7% compared with the control group without GBFS, which might be due to the different particle properties of FA and

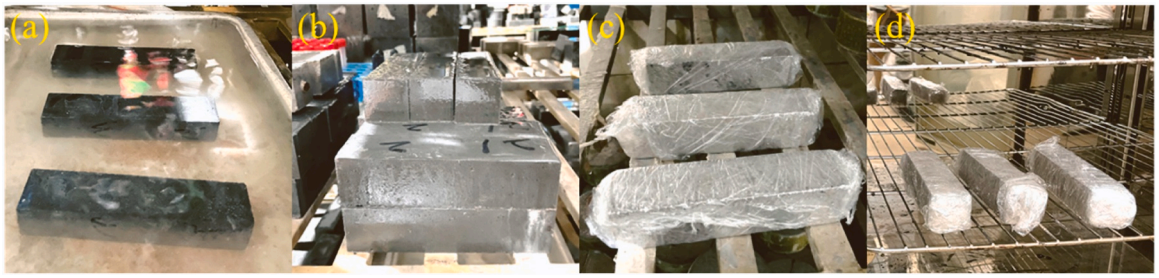

Fig. 4. Mortar samples cured by different methods, (a) water curing, (b) standard curing, (c) sealed curing, (d) heat curing.

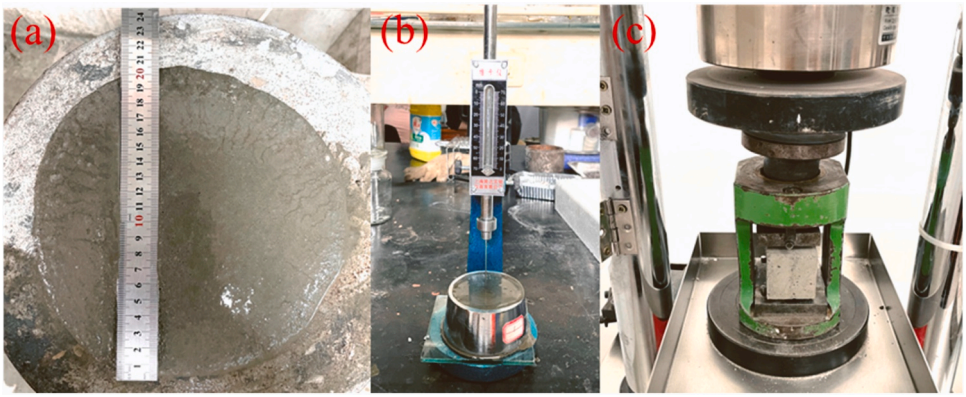

Fig. 5. Working performance test of the geopolymers, (a) fluidity, (b) setting time, (c) compressive strength.

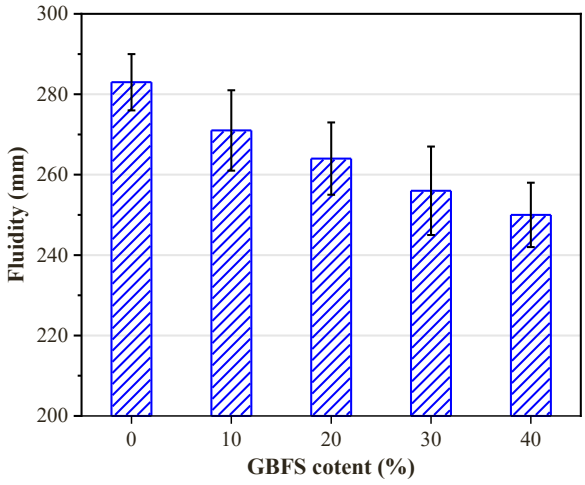

Fig. 6. The fluidity of geopolymers with different GBFS content.

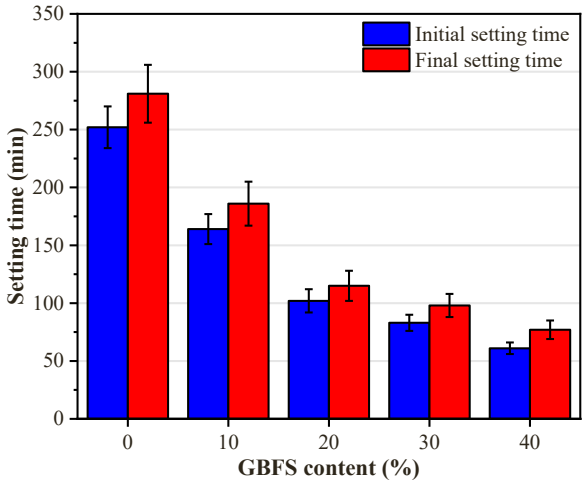

Fig. 7. Setting time of geopolymers with different GBFS content.

GBFS. Previous studies[4,49,53] have shown that the FA particles exhibit a spherical morphology and possess smooth surfaces, resulting in low interparticle friction. In contrast, the particles of GBFS exhibit an irregular shape, contributing to a high degree of friction between particles. Therefore, when the content of GBFS increased and the content of FA decreased, the viscous resistance of the particles inside the mixture increased, which ultimately led to a decrease in fluidity, which is consistent with the study results of Guo et al.[17].

3.1.2. *Setting time*

The connection between the setting time and the GBFS content is presented in Fig. 7. As GBFS content increased, there is a notable reduction in setting time of the geopolymer paste. The initial setting time of the geopolymer paste was shortened from 252 min to 61 min when the GBFS content was increased from 0% to 40%, which was reduced by 76%, and the geopolymer paste's final setting time was shortened from 281 min to 77 min, which was reduced by 73%. The solidification of geopolymer is determined by the network-like aluminosilicate gel produced by the condensation reaction of silica-aluminum constituents under alkali activation. For geopolymers, the reactivity of FA is lower than that of GBFS, and the early hydration is slower [54]. However, due to the high-amount of CaO in GBFS (40.42%), in the geopolymer paste, the incorporation of GBFS may speed up the development of calcium silicate hydrate (C-S-H) gel and calcium aluminosilicate hydrate (C-A-S-H) gel, thus accelerating solidification to shorten setting time.

3.1.3. Compressive strength

Fig. 8. displays the compressive strength at 3d, 7d, and 28d for mortar samples under different GBFS content and curing conditions. As depicted in Fig. 8(a), it is evident that as GBFS content improved, the compressive strength improved as well. When the dosage of GBFS rose from 0% to 40%, the 3d, 7d and 28d compressive strength of geopolymer mortar increased from 9.2 MPa, 15.5 MPa and 31.9–34.7 MPa, 53.4 MPa and 60.6 MPa, respectively. According to previous studies [44,55], the CaO content in traditional geopolymer precursors (such as FA and metakaolin) is low, and the three-dimensional network of aluminosilicate gel produced by geopolymerization determines the strength. However, the findings of Kim et al.[37] showed that the high-amount of CaO in GBFS may result in more C-S-H gel and C-A-S-H gel in slurry with the addition of GBFS, which may accelerate the development of early strength. Therefore, with the increase of GBFS content from 0% to 40%, the 3d compressive strength of geopolymer mortar reached 28.8%, 31.5%, 42.6%, 45.4% and 57.3% of the 28d compressive strength, respectively, the 7d compressive strength reached 48.6%, 57.3%, 63.3%, 80.0% and 88.1% of the 28d compressive strength, respectively, which represented a significant acceleration in the development of early strength. Additionally, it has been reported that GBFS possesses a nucleation effect [56], and higher amounts of GBFS will provide additional nucleation sites for slurry, encouraging the development of C-S-H gel and C-A-S-H gel, consequently improving geopolymers' compressive strength.

Fig. 8(b) depicts the impact of various curing methods on the compressive strength of mortar samples. The 28d compressive strength of mortar samples at the curing temperature of 20 ℃ is in the following order: GW30 (water curing), GS30 (sealed curing) and GST30 (standard curing), with values of 57.5 MPa, 68 MPa, and 70.8 MPa, respectively. Water curing will dissolve the alkali within the mortar into water, resulting in a lack of alkali inside the mortar to dissociate the aluminosilicate glass body, so that there are not enough Si and Al monomers for geopolymerisation. Therefore, the compressive strength of GW30 is the lowest. Sealing curing will isolate the mortar samples from the external water. With the continuous progress of geopolymerisation and hydration in geopolymer mortars, there is a lack of water inside the mortar, thus slowing down the development of compressive strength. Standard curing provides enough water for geopolymerisation and hydration, and the alkali in mortars will not be diluted by water. Therefore, mortar samples have the highest compressive strength under standard curing condition. The results are similar to the findings of Manojsuburam et al.[57]. The early strength development of geopolymers benefits from the high-temperature conditions. Compared with other curing methods, heat curing has the highest early compressive strength while later strength increase is slowly. The 3d compressive strength of GH30_60C_24h (heat curing) is 63.5 MPa, which is 74.9% higher than that of GST30 (standard curing), but its 28d compressive strength (76.3 MPa) is only 20.2% higher than 3d compressive strength.

Fig. 8(c) illustrates the compressive strength after heat curing for 24 h at various temperatures. The results demonstrated that as the temperature climbed from 20 °C to 60 °C, the geopolymer mortar's

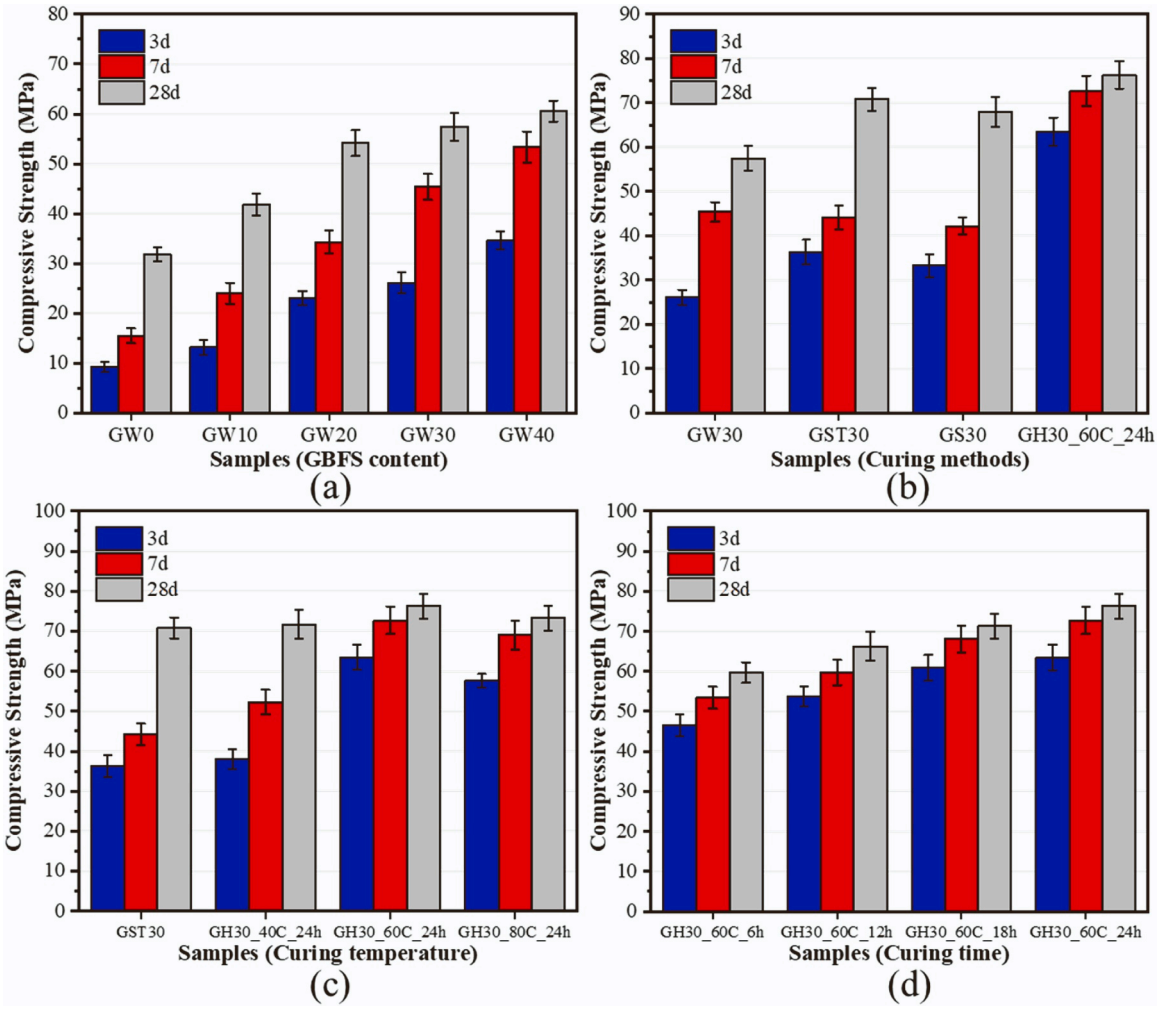

Fig. 8. The 3d, 7d and 28d compressive strength of mortar samples under different GBFS content and curing conditions, (a) GBFS content, (b) curing methods, (c) curing temperature, (d) curing time.

compressive strength increased, and higher curing temperatures are responsible for the greater early strength, which is consistent with the findings of Kong et al.[48]. The 3d compressive strength of GST30 is only 51.3% of its 28d compressive strength, whereas the 3d compressive strength of GH30_60C_24h reaches 83.2% of its 28d compressive strength. With temperature rose to 80 °C, however, the compressive strength began to decrease. The 28d compressive strength of GH30_80C_24h was 3 MPa lower than that of GH30_60C_24h, which may be due to the increase of shrinkage cracks within the mortar samples under excessively high temperatures, thereby negatively impacting the compressive strength [58]. Therefore, for the ternary geopolymer prepared in this paper, it is recommended that the maximum curing temperature should not exceed 60 °C.

The compressive strength after heat curing under 60 °C for various periods is depicted in Fig. 8(d). Similar to raising the curing temperature, the compressive strength can be enhanced by prolonging curing period. The 3d compressive strength of GH30_60C_24h is 36.6% higher than GH30_60C_6h, and the 28d compressive strength of GH30_60C_24h is 27.8% higher than GH30_60C_6h. When the heat curing time exceeded 18 h, prolonging the curing time had less of an impact. The 3d compressive strength of GH30_60C_24h is only 4.3% higher than that of GH30_60C_18 h. This may be because the long-term heat curing induces the drying shrinkage of the mortar, resulting in shrinkage cracks inside the mortar. Therefore, for the ternary geopolymer prepared in this study, it is suggested that the curing time at 60 °C should not exceed 18 h.

3.2. Microscopic analysis

3.2.1. XRD analysis

Fig. 9 presents the XRD patterns of paste samples after 3d of curing under different GBFS content and curing methods. The results revealed that the primary mineral phases of the seven groups were mullite (Al_2O_3), quartz (SiO_2), C-A-S-H gel, CSH gel and RO phase. Mullite was the mineral phase existed in FA, and quartz was from FA and GBFS. RO phase was the mineral phase derived from SS, which was formed by high-temperature solid solution of metal oxides and did not participate in the geopolymerisation. The presence of mullite phase and quartz phase in GW0 indicates that the original mineral phase of FA still exists in the geopolymer, which means that when SS:FA:GBFS= 5:5:0, FA in the samples does not fully participate in the geopolymerisation. However, the mullite peak and quartz peak at 2θ= 16° and 2θ= 20° did not appear when SS:FA:GBFS= 5:2:3, and there was a significant decrease in the quartz peak's intensity at 2θ= 26°, indicating that GBFS contributed to improve the reaction degree of precursors, thereby consuming SiO_2 in FA and GBFS, which was similar with the findings of Long et al. [59].

Existing works show that the incorporation of Ca-rich materials (such as GBFS and SS) to geopolymer precursors leads to the hydration of Ca components under alkaline conditions, which contributes to the generation of C-S-H and C-A-S-H [60]. As amorphous phases, C-S-H and C-A-S-H exist as zeolite-like structures in geopolymers, which cannot exhibit strong Bragg reflections [55]. In Fig. 9, these phases are represented by broad humps around 2θ= 28–35°. It can be observed that except for the control group GW0, all other groups exhibited diffraction peaks corresponding to C-S-H phase at 2θ= 29°, which indicated that the addition of GBFS promoted the generation of C-S-H. In addition, the peak intensity of mortar samples (GH30_60C_24h, GH30_80C_24h and GH30_60C_12h) cured at high temperature increased at 2θ= 29°, which proved that the hydration reaction of geopolymer precursors was accelerated by high-temperature curing.

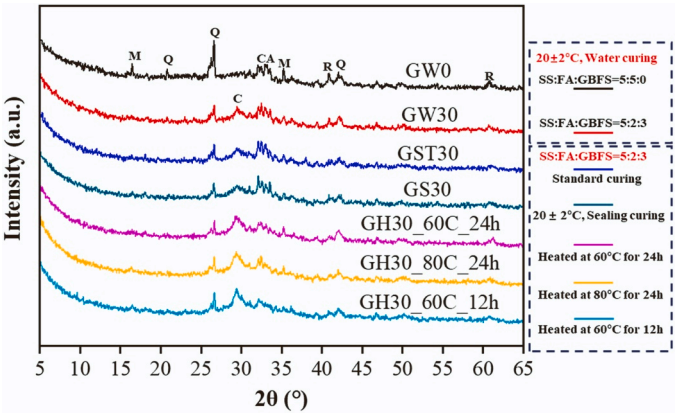

Fig. 9. XRD patterns of seven groups of geopolymer pastes, M=Mullite, Q=Quartz, CA=C-A-S-H, C= C-S-H, R=RO phase.

3.2.2. FTIR analysis

Fig. 10 displays the FTIR spectra of paste samples after 28d of curing under different GBFS content and curing conditions. The stretching and bending vibrations of the O-H bonds are responsible for the absorption spikes at wavenumbers approximately 3459 and 1646 cm^{-1}, respectively, which confirms the existence of bound water in the gel and further demonstrates the production of hydration products. Additionally, the absorption spike at 979 cm^{-1} is generated by the asymmetric stretching vibration of the Si-O-Si (Al) bonds, whereas absorption spikes at 451 and 674 cm^{-1} are generated by the bending vibrations of the Si-O-Si bonds. The existence of these three characteristic spikes signifies the formation of C-(A)-S-H gel. The Al-O bonds' vibration is represented by the absorption spike around 719 cm^{-1}. The absorption spikes at 1426 and 1488 cm^{-1} represented the bending vibrations of C-O bonds, implying the existence of carbonate products in the samples, possibly arising from carbonation. However, the relatively weak intensities of these two absorption spikes suggest that the samples contain only a small amount of carbonate. In agreement with the findings of the XRD, indicating that the ternary geopolymer obtained in this study is relatively difficult to carbonate, which is possibly due to the densely packed arrangement of reaction products, rendering the structure of the geopolymer highly compact and hindering the penetration of CO_2 into the sample's interior.

3.2.3. TG-DTG analysis

Fig. 11 shows the TG-DTG curves of paste samples with different GBFS contents and curing conditions after curing for 28d. According to the conclusions of Shi et al. [61], the weight loss of GBFS materials with alkali activation between 20 and 200 °C represented the decomposition of C-(A)-S-H gel. Similarly, the research by Guo et al. indicated that

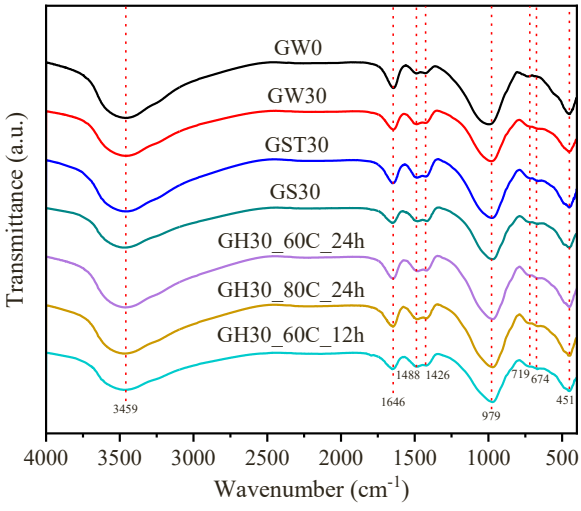

Fig. 10. FTIR spectra of paste samples after 28d of curing under different GBFS content and curing conditions.

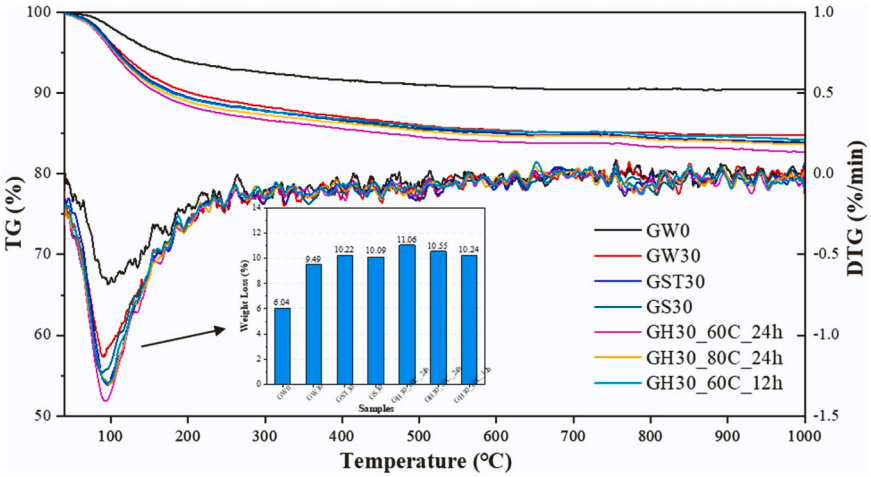

Fig. 11. TG-DTG curves of the paste samples with different GBFS contents and curing conditions after curing for 28d.

C-(A)-S-H gel tends to decompose within the temperature range of 20–200 °C [17]. Therefore, the weight loss of the paste samples within the temperature of 20–200 °C reflects the quantity of C-(A)-S-H generated through geopolymerisation and hydration. It can be observed from Fig. 11 that the weight losses of GW0, GW30, GST30, GS30, GH30_60C_24h, GH30_80C_24h and GH30_60C_12h at 20–200 °C are 6.04%, 9.49%, 10.22%, 10.09%, 11.05%, 10.55%, and 10.24%, respectively. The weight loss of GW30 increased by 57.1% in comparison to GW0 as the GBFS content rose from 0% to 30%, indicating a significant increase of the C-(A)-S-H gel content. This explains the enhancement of compressive strength after the doping of GBFS. The variation in C-(A)-S-H gel content is closely linked to the changes in compressive strength. The weight loss of the samples cured under different conditions from high to low is heat curing, standard curing, sealing curing and water curing, which agrees with the order of compressive strength in 3.1.3, confirming that appropriate heat curing can accelerate the hydration and geopolymerisation, thereby increasing the content of C-(A)-S-H gel in the geopolymer and consequently improving its strength. However, Schöler et al. pointed out that excessively high temperatures would make the hydration products cover rapidly on the particles' surface and hinder the hydration reaction [62]. Therefore, as the curing temperature rose to 80 °C, the rapidly generated C-(A)-S-H gel will cover the surface of FA, GBFS and SS, thereby reducing the contact area between geopolymer precursor and alkali activator [61], resulting in a decrease in the amount of C-(A)-S-H gel, which explains why the weight loss of GH30_80C_24h (10.55%) is lower than that of GH30_60C_24h (11.06%).

3.2.4. SEM-EDS analysis

Fig. 12 shows the SEM images of geopolymer pastes after curing for 3 days. Compared with GW30, it can be clearly observed that the structure of GW0 is notably looser, and contains many unhydrated FA particles, resulting in its lower compressive strength. When the content of GBFS increased to 30%, the geopolymer precursor produced more matrix gels through geopolymerisation and hydration, and the number of unhydrated FA particles in GW30 was reduced. Therefore, the 28d compressive strength of GW30 (57.5 MPa) is much higher than that of GW0 (31.9 MPa). The results indicate that FA exhibits lower reactivity, thus it cannot fully participate in the geopolymerisation. However, When GBFS is used to replace FA, the addition of GBFS has an activation effect on SS and FA due to the large amount of highly active CaO, SiO_2 and Al_2O_3 in GBFS, which accelerates the geopolymerisation and hydration. So, the compressive strength of geopolymer mortar increased with the increase of GBFS content. In addition, due to the high-amount of CaO in SS and GBFS, the Ca / (Si + Al) ratio in GW30 is significantly higher than that in GW0. It has been reported that the environment with a higher Ca / (Si + Al) ratio is favorable for the formation of needle-like C-S-H [59]. As shown in Fig. 12(b), these needle-like C-S-H fill the pores and voids, consequently enhancing the compressive strength of the geopolymers.

Fig. 12(b), (c), (d), and (e) show that the ultrastructure of the geopolymer is significantly impacted by various curing methods. Due to the dilution of alkali activator and the consumption of water under water curing and sealed curing, the reaction of geopolymer precursor is not complete, resulting in fewer gels formed by geopolymerisation and hydration. The matrix gel produced by geopolymer precursors increases under standard curing, forming a uniform gel network within the geopolymer. Therefore, at room temperature, the geopolymer mortar with standard curing has the highest compressive strength. The high temperature increases the reaction degree and reaction speed of geopolymer precursors under heat curing, a large number of reaction products fill the pores and defects of the geopolymer, which results in a denser microstructure. This is why heat curing can significantly enhance the compressive strength of geopolymer mortar. However, Fig. 12(f) shows that after raising the temperature to 80 °C, the rapid consumption of free water at high temperatures may result in more shrinkage cracks in the geopolymer. Shrinkage cracks will reduce the structural stability of geopolymers, thereby reducing the compressive strength of geopolymers. Therefore, as the curing temperature increased from 60 °C to 80 °C, the 28d compressive strength of GH30_80C_24h (69 MPa) is lower than that of GH30_60C_24h (72.7 MPa).

Fig. 12(g) and (h) illustrate the layered reaction products similar to hydrotalcite observed in GH30_60C_24h. GBFS and SS accounted for 80% of the total weight of geopolymer precursors in GH30_60C_24h. XRF results showed that the content of MgO in GBFS and SS was 7.4% and 3.85%, respectively. Under alkaline conditions, Mg^{2+} leaches out from GBFS and SS and reacts with the aluminum components in FA and GBFS, forming layered Mg-Al bimetallic hydroxides within the geopolymer. It has been reported that hydrotalcite-like compounds contribute to the resorption and immobilization of heavy metal ions in the environment [63], thereby enhancing the environmental performance of geopolymers.

To verify the different reaction products in Fig. 12, the backscattered electron (BSE) EDS images of GW0 and GH30_60C_24h are presented in Fig. 13. Fig. 13(a) illustrates the presence of unreacted SS and FA within GW0. Due to FA's relatively low reactivity, just a little of N-A-S-H gel is formed when the silicon-aluminum component of FA interacts with Na+ from the water glass. The gel in GW0 is mainly composed of C-S-H gel formed by hydration of calcium component in SS. With the addition of GBFS, the reaction degree of FA and SS increased under the activation of GBFS. As shown in Fig. 13(b), no unhydrated FA and SS particles were found in GH30_60C_24h, but there were unhydrated GBFS particles. This

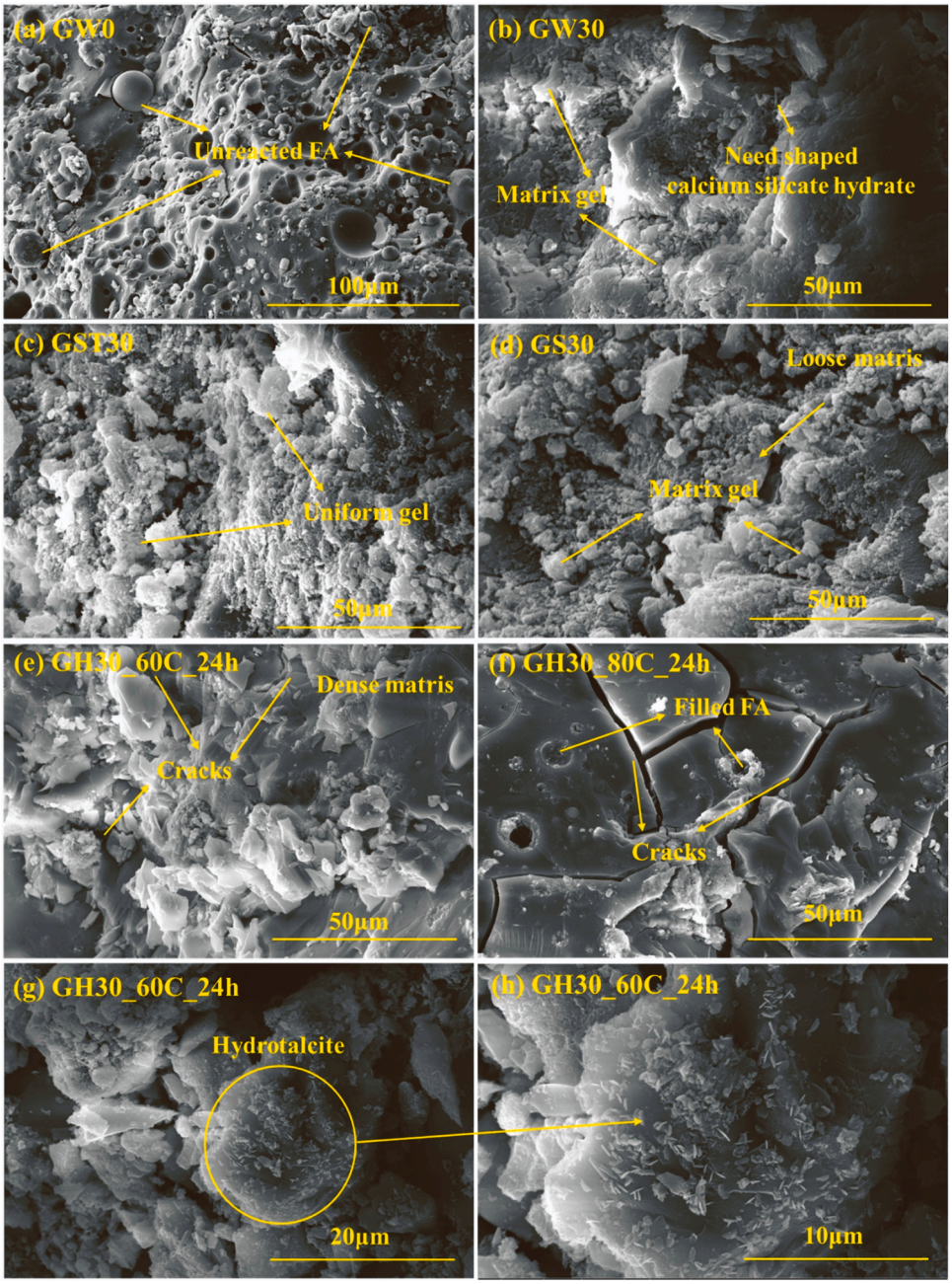

Fig. 12. SEM images of geopolymer pastes after curing for 3 days, (a) GW0, (b) GW30, (c) GST30, (d) GS30, (f) GH30_80C_24h, (e), (g) and (h) GH30_60C_24h.

could be illustrated by the quick development of C-(A)-S-H gel at higher temperatures, which encapsulates the GBFS particles and hinders further reactions. The gel composition within GH30_60C_24h primarily consists of C-(A)-S-H gel, accompanied by a small amount of N-A-S-H gel. These two gel products, along with hydrotalcite, collectively constitute the microstructure of the geopolymer. Therefore, the reaction products in GH30_60C_24h are more continuous, uniform, and have fewer pores and defects compared to GW0. Consequently, GH30_60C_24h demonstrates higher compressive strength than GW0.

3.2.5. *Hydration process of SS-FA-GBFS ternary geopolymer*

According to the results of the above tests, the hydration process of SS-FA-GBFS ternary geopolymer can be summarized as follows:

1. When the geopolymer precursor does not contain GBFS, in an alkaline environment, the glass body in SS and FA are dissolved, and the SiO_2 and Al_2O_3 in SS and FA react with OH^- to form $[H_3SiO_4]^-$, $[H_3AlO_4]^{2-}$ and $[Al(OH)_6]^{3-}$ as monomers for the geopolymerisation, as shown in Eqs. (3), (4), and (5).

$$SiO_2 + OH^- + H_2O \rightarrow [H_3SiO_4]^- \quad (3)$$

$$AlO_2^- + OH^- + H_2O \rightarrow [H_3AlO_4]^{2-} \quad (4)$$

$$AlO_2^- + OH^- + H_2O \rightarrow [AlOH_6]^{3-} \quad (5)$$

2. $[H_3SiO_4]^-$ and $[H_3AlO_4]^{2-}$ reacts with Na^+ in water glass to form N-A-S-H gel, while the Ca^{2+} reacts with water to form $Ca(OH)_2$, which subsequently reacts to form C-S-H gel, as depicted in Eqs. (6) and (7). Due to the lower reactivity of SS and FA, the amount of gel formed in the system at this stage is relatively limited.

$$Na^+ + [H_3SiO_4]^- + [H_3AlO_4]^{2-} \rightarrow N-A-S-H \quad (6)$$

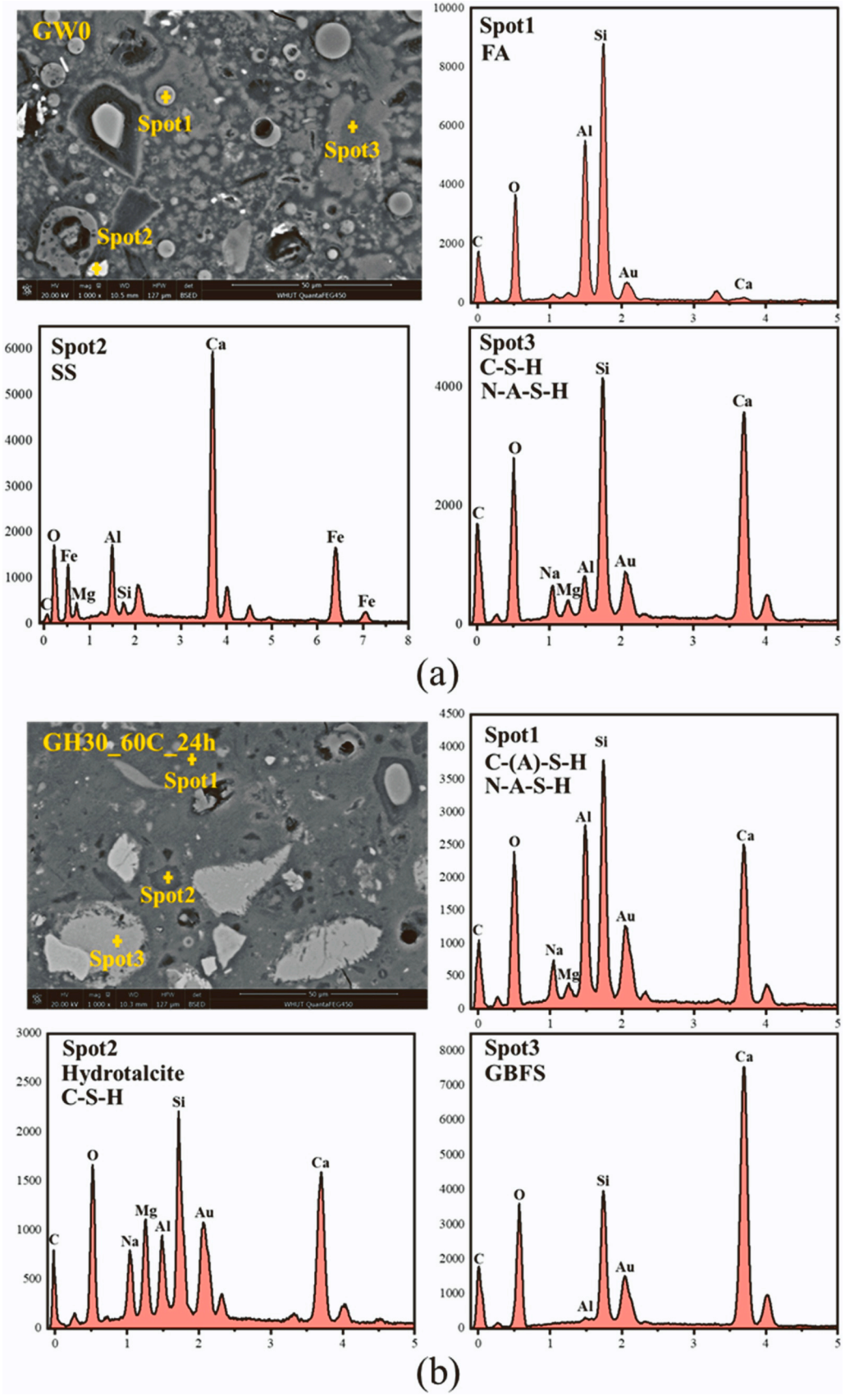

Fig. 13. EDS images of GW0 and GH30_60C_24h, (a) GW0, (b) GH30_60C_24h.

$$mCa(OH)_2 + SiO_2 + H_2O \rightarrow C-S-H \quad (7)$$

3. With the addition of GBFS, the reactive components such as CaO, SiO_2, and Al_2O_3 in GBFS has an activation effect on both SS and FA, thereby accelerating the hydration and geopolymerisation in the geopolymer slurry. At this stage, the substantial presence of Ca^{2+}, $[H_3AlO_4]^{2-}$, and $[H_3SiO_4]^-$ in the system leads to significant generation of C-(A)-S-H gel. Additionally, Mg^{2+} in GBFS and SS reacts with $[AlOH_6]^{3-}$to form hydrotalcite, as shown in Eqs. (8) and (9).

$$Ca^+ + [H_3SiO_4]^- + [H_3AlO_4]^{2-} \rightarrow C-(A)-S-H \quad (8)$$

$$6Mg^{2+} + 2[AlOH_6]^{3-} + CO_3{}^{2-} + 4OH^- + H_2O \rightarrow 6MgO{\cdot}Al_2O_3{\cdot}CO_2{\cdot}12H_2O \quad (9)$$

4. The C-(A)-S-H gel and N-A-S-H gel were connected to form a gel network, resulting in an improvement in geopolymer's strength. During the heat curing, the reaction of the geopolymer precursor is accelerated, and the network-like reaction products generated by geopolymerisatio are continuously arranged and accumulated, and finally a highly dense microstructure is formed. Only a small part of the unreacted $Ca(OH)_2$ reacts with CO_2 to form $CaCO_3$, which is why the diffraction peaks and thermolysis of calcite are difficult to observe in the XRD and FTIR results.

4. Conclusions

In this study, a high-strength ternary geopolymer was synthesized using SS, FA, and GBFS as precursors. The influence of GBFS content and curing methods on the mechanical properties, microstructure, and reaction products of the geopolymer with high SS content (50%) were investigated. Through the working performance and microscopic characteristics of geopolymers, the following conclusions can be drawn:

(1) The incorporation of GBFS improves the compressive strength of geopolymers while reducing its setting time and fluidity, but the working performance of the geopolymers was acceptable. When SS content reached 50%, as the dosage of GBFS rose from 0% to 40%, geopolymers' 28d compressive strength increased from 31.9 MPa to 60.6 MPa.
(2) At room temperature, geopolymer mortars under standard curing conditions exhibited the highest compressive strength, followed by sealed and water curing. Appropriate heat curing can accelerate the formation of gels and contribute to improve the compressive strength of geopolymers. However, excessive curing temperatures or curing time will lead to the formation of shrinkage cracks, resulting in a decrease of compressive strength.
(3) Microscopic analysis indicated that the reaction product was mainly C-(A)-S-H gel, The geopolymers' compressive strength has a high correlation with the thermal decomposition weight loss of C-(A)-S-H gel. Heat curing can improve the reaction degree of geopolymer precursors, but under excessively high temperature, the precursor particles will be covered by the rapidly generated reaction products and cannot continue to participate in the reaction.
(4) The SEM-EDS results demonstrate that under heat curing conditions, the continuous aggregation of reactive monomers in the slurry forms a three-dimensional aluminosilicate network structure, which further arranges and stacks, resulting in a geopolymer with a denser microstructure and more uniform reaction products. The Mg^{2+} in SS and GBFS will react with the aluminum components under the alkaline environment to generate hydrotalcite, further enhancing the geopolymer's structural stability.
(5) The developed ternary geopolymer achieves high-content utilization of SS in geopolymers, thereby increasing the utilization rate of SS in China and reducing its environmental pollution. In practical applications, standard curing, water curing, and sealed curing are suitable curing conditions for most industrial scenarios, while heat curing is beneficial for improving the early strength of geopolymer.

5. Future recommendation

Despite the potential benefits of using FA, SS, and GBFS to produce geopolymers, such as reducing cement consumption and promoting the recycling of solid waste, there remain uncertainties regarding the economic and environmental viability of geopolymers due to their heavy reliance on industrial water glass as an alkali activator. Therefore, a comprehensive life cycle assessment of these waste solid-based cementitious materials is essential. In addition, SS, GBFS and FA all contain a variety of heavy metal ions, so it is essential to test the leaching toxicity of solid waste-based geopolymers, which will be carried out in the ongoing research. Furthermore, the hydration kinetics and ion migration of ternary geopolymers will be studied to better understand the hydration mechanism of SS-based geopolymers.

CRediT authorship contribution statement

Xinkui Yang: Investigation, Conceptualization, Methodology, Writing – original draft. **Shaopeng Wu:** Project administration, Supervision. **Shi Xu:** Investigation, Formal analysis. **Boyu Chen:** Investigation, Formal analysis. **Dongyu Chen:** Investigation, Writing – review & editing. **Fusong Wang:** Conceptualization, Writing – review & editing. **Jian Jiang:** Conceptualization. **Lulu Fan:** Writing – review & editing. **Liangliang Tu:** Writing – review & editing.

Declaration of Competing Interest

The authors declare that they have no known competing financial interests or personal relationships that could have appeared to influence the work reported in this paper.

Data availability

Data will be made available on request.

Acknowledgments

This work was supported by the National Natural Science Foundation of China (No. 52308464), Hubei Science and Technology Innovation Talent and Service Project (No. 2022EHB006), State Key Laboratory of Silicate Materials for Architectures (Wuhan University of Technology) (SYSJJ2023–05), 2021AB26023 Key R&D Program of Guangxi Province (No. 2021AB26023).

References

[1] F. Gu, J. Xie, C. Vuye, Y. Wu, J. Zhang, Synthesis of geopolymer using alkaline activation of building-related construction and demolition wastes, J. Clean. Prod. (2023), 138335.
[2] O. Shee-Ween, H. Cheng-Yong, L. Yun-Ming, M. Mustafa Al Bakri Abdullah, H. Li-Ngee, P. Pakawanit, M. Suhaimi Khalid, W. Hazim Bin Wan Muhammad, O. Wan-En, H. Yong-Jie, N. Yong-Sing, N. Hui-Teng, Green development of fly ash geopolymer via casting and pressing Approaches: Strength, Morphology, efflorescence and Ecological Properties, Constr. Build. Mater. 398 (2023), 132446.
[3] H. Wu, C. Liang, D. Yang, Z. Ma, Development of sustainable geopolymer materials made with ground geopolymer waste powder as renewable binder up to 100%, Constr. Build. Mater. 400 (2023), 132746.
[4] G.L. Golewski, Combined Effect of Coal Fly Ash (CFA) and Nanosilica (nS) on the Strength Parameters and Microstructural Properties of Eco-Friendly Concrete, Energies 16 (1) (2023) 452.
[5] G.L. Golewski, Examination of water absorption of low volume fly ash concrete (LVFAC) under water immersion conditions, IOP Publishing Ltd.
[6] G.L. Golewski, The effect of the addition of coal fly ash (CFA) on the control of water movement within the structure of the concrete, Materials 16 (15) (2023) 5218.

[7] G.L. Golewski, Assessing of water absorption on concrete composites containing fly ash up to 30% in regards to structures completely immersed in water, Case Stud. Constr. Mater. 19 (2023), e02337.
[8] N.S. Piro, A.S. Mohammed, S.M. Hamad, Evaluate and predict the resist electric current and compressive strength of concrete modified with GGBS and steelmaking slag using mathematical models, J. Sustain. Metall. 9 (1) (2023) 194–215.
[9] N.S. Piro, A.S. Mohammed, S.M. Hamad, The impact of GGBS and ferrous on the flow of electrical current and compressive strength of concrete, Constr. Build. Mater. 349 (2022), 128639.
[10] M.S. Barkhordari, D.J. Armaghani, A.S. Mohammed, D.V. Ulrikh, Data-Driven Compressive Strength Prediction of Fly Ash Concrete Using Ensemble Learner Algorithms, Buildings 12 (2) (2022) 132.
[11] A. Mohammed, R. Kurda, D.J. Armaghani, M. Hasanipanah, Prediction of compressive strength of concrete modified with fly ash: Applications of neuro-swarm and neuro-imperialism models, Comput. Concr. 5 (2021) 27.
[12] H.U. Ahmed, R.R. Mostafa, A. Mohammed, P. Sihag, A. Qadir, Support vector regression (SVR) and grey wolf optimization (GWO) to predict the compressive strength of GGBFS-based geopolymer concrete, Neural Comput. Appl. 35 (3) (2023) 2909–2926.
[13] H.U. Ahmed, A.A. Mohammed, A. Mohammed, Soft computing models to predict the compressive strength of GGBS/FA- geopolymer concrete, PLOS ONE 17 (5) (2022), e0265846.
[14] D. Kakasor Ismael Jaf, A.S. Abdulrahman, P.I. Abdulrahman, A. Salih Mohammed, R. Kurda, H.U. Ahmed, R.H. Faraj, Effitioned soft computing models to evaluate the impact of silicon dioxide (SiO2) to calcium oxide (CaO) ratio in fly ash on the compressive strength of concrete, J. Build. Eng. 74 (2023), 106820.
[15] A.G. Borçato, M. Thiesen, R.A. Medeiros-Junior, Mechanical properties of metakaolin-based geopolymers modified with different contents of quarry dust waste, Constr. Build. Mater. 400 (2023), 132854.
[16] Z. Li, Z. Xiong, B. Zhang, D. Huang, J. Huang, L. Yan, L. Li, Seawater used to Metakaolinite-based geopolymer preparation, Constr. Build. Mater. 392 (2023), 131816.
[17] L. Guo, M. Zhou, X. Wang, C. Li, H. Jia, Preparation of coal gangue-slag-fly ash geopolymer grouting materials, Constr. Build. Mater. 328 (2022), 126997.
[18] N. Mao, D. Wu, K. Chen, K. Cao, J. Huang, Combining experiments and molecular dynamics simulations to investigate the effects of water on the structure and mechanical properties of a coal gangue-based geopolymer, Constr. Build. Mater. 389 (2023), 131556.
[19] V. Revilla-Cuesta, M. Skaf, A. Santamaría, J.M. Romera, V. Ortega-López, Elastic stiffness estimation of aggregate–ITZ system of concrete through matrix porosity and volumetric considerations: explanation and exemplification, Arch. Civ. Mech. Eng. 22 (2) (2022) 59.
[20] B. Bai, F. Bai, Q. Nie, X. Jia, A high-strength red mud–fly ash geopolymer and the implications of curing temperature, Powder Technol. 416 (2023), 118242.
[21] H. Majdoubi, R. Makhlouf, Y. Haddaji, M. Nadi, S. Mansouri, N. Semllal, M. Oumam, B. Manoun, J. Alami, H. Hannache, Y. Tamraoui, Valorization of phosphogypsum waste through acid geopolymer technology: synthesis, characterization, and environmental assessment, Constr. Build. Mater. 371 (2023), 130710.
[22] X. Li, H. Mehdizadeh, T.-C. Ling, Environmental, economic and engineering performances of aqueous carbonated steel slag powders as alternative material in cement pastes: Influence of particle size, Sci. Total Environ. (2023), 166210.
[23] C. Yang, S. Wu, P. Cui, S. Amirkhanian, Z. Zhao, F. Wang, L. Zhang, M. Wei, X. Zhou, J. Xie, Performance characterization and enhancement mechanism of recycled asphalt mixtures involving high RAP content and steel slag, J. Clean. Prod. 336 (2022), 130484.
[24] J. Li, J. Yu, S. Wu, J. Xie, The mechanical resistance of asphalt mixture with steel slag to deformation and skid degradation based on laboratory accelerated heavy loading test, Mater. (Basel, Switz.) 15 (3) (2022).
[25] Z. Zhao, Z. Wang, S. Wu, J. Xie, C. Yang, N. Li, P. Cui, Road performance, VOCs emission and economic benefit evaluation of asphalt mixture by incorporating steel slag and SBS/CR composite modified asphalt, Case Stud. Constr. Mater. 18 (2023), e01929.
[26] P. Cui, S. Wu, Y. Xiao, R. Hu, T. Yang, Environmental performance and functional analysis of chip seals with recycled basic oxygen furnace slag as aggregate, J. Hazard. Mater. 405 (2021), 124441.
[27] Y. Lv, S. Wu, P. Cui, Q. Liu, Y. Li, H. Xu, Y. Zhao, Environmental and feasible analysis of recycling steel slag as aggregate treated by silicone resin, Constr. Build. Mater. 299 (2021), 123914.
[28] S. Zhang, D. Niu, Hydration and mechanical properties of cement-steel slag system incorporating different activators, Constr. Build. Mater. 363 (2023), 129981.
[29] Y. Rui, C. Qian, CO_2-fixing steel slag on hydration characteristics of cement-based materials, Constr. Build. Mater. 354 (2022), 129193.
[30] V. Ortega-López, V. Revilla-Cuesta, A. Santamaría, A. Orbe, M. Skaf, Microstructure and Dimensional Stability of Slag-Based High-Workability Concrete with Steelmaking Slag Aggregate and Fibers, J. Mater. Civ. Eng. 34 (9) (2022), 04022224.
[31] A. Santamaría, V. Revilla-Cuesta, M. Skaf, J.M. Romera, Full-scale sustainable structural concrete containing high proportions of by-products and waste, Case Stud. Constr. Mater. 18 (2023), e02142.
[32] V. Revilla-Cuesta, M. Skaf, V. Ortega-López, J.M. Manso, Multi-parametric flowability classification of self-compacting concrete containing sustainable raw materials: An approach to real applications, J. Build. Eng. 63 (2023), 105524.
[33] X. Guo, J. Yang, Intrinsic properties and micro-crack characteristics of ultra-high toughness fly ash/steel slag based geopolymer, Constr. Build. Mater. 230 (2020), 116965.
[34] T. Bai, Z.-G. Song, Y.-G. Wu, X.-D. Hu, H. Bai, Influence of steel slag on the mechanical properties and curing time of metakaolin geopolymer, Ceram. Int. 44 (13) (2018) 15706–15713.
[35] W. Song, Z. Zhu, Y. Peng, Y. Wan, X. Xu, S. Pu, S. Song, Y. Wei, Effect of steel slag on fresh, hardened and microstructural properties of high-calcium fly ash based geopolymers at standard curing condition, Constr. Build. Mater. 229 (2019), 116933.
[36] X. Zhu, W. Li, Z. Du, S. Zhou, Y. Zhang, F. Li, Recycling and utilization assessment of steel slag in metakaolin based geopolymer from steel slag by-product to green geopolymer, Constr. Build. Mater. 305 (2021), 124654.
[37] G.W. Kim, T. Oh, S. Kyun Lee, N. Banthia, D.-Y. Yoo, Development of Ca-rich slag-based ultra-high-performance fiber-reinforced geopolymer concrete (UHP-FRGC): Effect of sand-to-binder ratio, Constr. Build. Mater. 370 (2023), 130630.
[38] M.S. Saif, M.O.R. El-Hariri, A.I. Sarie-Eldin, B.A. Tayeh, M.F. Farag, Impact of Ca+ content and curing condition on durability performance of metakaolin-based geopolymer mortars, Case Stud. Constr. Mater. 16 (2022), e00922.
[39] B. Ma, Z. Zhu, W. Huo, L. Yang, Y. Zhang, H. Sun, X. Zhang, Assessing the viability of a high performance one-part geopolymer made from fly ash and GGBS at ambient temperature, J. Build. Eng. 75 (2023), 106978.
[40] S. Saha, C. Rajasekaran, Enhancement of the properties of fly ash based geopolymer paste by incorporating ground granulated blast furnace slag, Constr. Build. Mater. 146 (2017) 615–620.
[41] U. Zakira, K. Zheng, N. Xie, B. Birgisson, Development of high-strength geopolymers from red mud and blast furnace slag, J. Clean. Prod. 383 (2023), 135439.
[42] M. Hongqiang, C. Hongyu, Z. Hongguang, S. yangyang, N. Yadong, H. Qingjie, H. Zetao, Study on the drying shrinkage of alkali-activated coal gangue-slag mortar and its mechanisms, Constr. Build. Mater. 225 (2019) 204–213.
[43] G. Kastiukas, S. Ruan, S. Liang, X. Zhou, Development of precast geopolymer concrete via oven and microwave radiation curing with an environmental assessment, J. Clean. Prod. 255 (2020), 120290.
[44] F.K. Alqahtani, K. Rashid, I. Zafar, M. Iqbal Khan, Assessment of morphological characteristics and physico-mechanical properties of geopolymer green foam lightweight aggregate formulated by microwave irradiation, J. Build. Eng. 35 (2021), 102081.
[45] M.-H. Nofalah, P. Ghadir, H. Hasanzadehshooiili, M. Aminpour, A.A. Javadi, M. Nazem, Effects of binder proportion and curing condition on the mechanical characteristics of volcanic ash- and slag-based geopolymer mortars; machine learning integrated experimental study, Constr. Build. Mater. 395 (2023), 132330.
[46] Y. Luo, S.H. Li, K.M. Klima, H.J.H. Brouwers, Q. Yu, Degradation mechanism of hybrid fly ash/slag based geopolymers exposed to elevated temperatures, Cem. Concr. Res. 151 (2022), 106649.
[47] Z. Hu, M. Wyrzykowski, P. Lura, Estimation of reaction kinetics of geopolymers at early ages, Cem. Concr. Res. 129 (2020), 105971.
[48] D.L.Y. Kong, J.G. Sanjayan, Effect of elevated temperatures on geopolymer paste, mortar and concrete, Cem. Concr. Res. 40 (2) (2010) 334–339.
[49] X. Guan, W. Luo, S. Liu, A.G. Hernandez, H. Do, B. Li, Ultra-high early strength fly ash-based geopolymer paste cured by microwave radiation, Dev. Built Environ. 14 (2023), 100139.
[50] A. Gultekin, K. Ramyar, Effect of curing type on microstructure and compressive strength of geopolymer mortars, Ceram. Int. 48 (11) (2022) 16156–16172.
[51] Z. Dong, H. Ma, W. Feng, Y. Nie, H. Shi, Achieving superior high-strength geopolymer via the synergistic effect of traditional oven curing and microwave curing, Constr. Build. Mater. 357 (2022), 129406.
[52] Y. Liu, Z. Zhang, G. Hou, P. Yan, Preparation of sustainable and green cement-based composite binders with high-volume steel slag powder and ultrafine blast furnace slag powder, J. Clean. Prod. 289 (2021), 125133.
[53] L. Ting, W. Qiang, Z. Shiyu, Effects of ultra-fine ground granulated blast-furnace slag on initial setting time, fluidity and rheological properties of cement pastes, Powder Technol. 345 (2019) 54–63.
[54] W. Feng, Y. Jin, D. Zheng, Y. Fang, Z. Dong, H. Cui, Study of triethanolamine on regulating early strength of fly ash-based chemically foamed geopolymer, Cem. Concr. Res. 162 (2022), 107005.
[55] S.A. Bernal, J.L. Provis, B. Walkley, R. San Nicolas, J.D. Gehman, D.G. Brice, A. R. Kilcullen, P. Duxson, J.S.J. van Deventer, Gel nanostructure in alkali-activated binders based on slag and fly ash, and effects of accelerated carbonation, Cem. Concr. Res. 53 (2013) 127–144.
[56] J.S.J. van Deventer, J.L. Provis, P. Duxson, G.C. Lukey, Reaction mechanisms in the geopolymeric conversion of inorganic waste to useful products, J. Hazard. Mater. 139 (3) (2007) 506–513.
[57] R. Manojsuburam, E. Sakthivel, E. Jayanthimani, A study on the mechanical properties of alkali activated ground granulated blast furnace slag and fly ash concrete, Mater. Today.: Proc. 62 (2022) 1761–1764.
[58] A. Dehghani, F. Aslani, N. Ghaebi, Panah, Effects of initial SiO2/Al2O3 molar ratio and slag on fly ash-based ambient cured geopolymer properties, Constr. Build. Mater. 293 (2021), 123527.
[59] Q. Long, Y. Liu, Q. Zhao, M. Zhou, B. Li, Effects of GGBFS:FA ratio and humid-heat-treating on the mechanical performance and microstructure of the steel slag-based ternary geopolymer, Constr. Build. Mater. 392 (2023), 131750.
[60] N.K. Lee, H.K. Lee, Setting and mechanical properties of alkali-activated fly ash/slag concrete manufactured at room temperature, Constr. Build. Mater. 47 (2013) 1201–1209.
[61] Y. Shi, Q. Zhao, C. Xue, Y. Jia, W. Guo, Y. Zhang, Y. Qiu, Preparation and curing method of red mud-calcium carbide slag synergistically activated fly ash-ground

granulated blast furnace slag based eco-friendly geopolymer, Cem. Concr. Compos. 139 (2023), 104999.
[62] A. Schöler, B. Lothenbach, F. Winnefeld, M. Zajac, Hydration of quaternary Portland cement blends containing blast-furnace slag, siliceous fly ash and limestone powder, Cem. Concr. Compos. 55 (2015) 374–382.
[63] B. Thangaraj, C. Jayaraj, G. V, S. Ayyamperumal, Silicate intercalated cobalt chromium–hydrotalcite (CoCr–HTSi): An environment-friendly recyclable catalyst for organic transformations, Catal. Commun. 74 (2016) 85–90.